Periodic magnetoconductance fluctuations in triangular quantum dots in the absence of selective probing

P. Bøggild, A. Kristensen, H. Bruus, S. M. Reimann, and P. E. Lindelof

Niels Bohr Institute, Ørsted Laboratory, University of Copenhagen, Universitetsparken 5, DK-2100 Copenhagen Ø, Denmark

We have studied the magnetoconductance of quantum dots with triangular symmetry and areas down to 0.2 μm^2, made in a high mobility two-dimensional electron gas embedded in a GaAs-Al$_x$Ga$_{1-x}$As heterostructure. Semiclassical simulations show that the gross features in the measured magnetoconductance are caused by ballistic effects. Below 1 K we observe a strong periodic oscillation, which may be explained in terms of the Aharanov-Bohm flux quantization through the area of a single classical periodic orbit. From a numerical and analytical analysis of possible trajectories in hard- and soft-walled potentials, we identify this periodic orbit as the enscribed triangle. Contrary to other recent experiments, this orbit is not accessible by classical processes for the incoming collimated beam. [S0163-1829(98)04924-8]

I. INTRODUCTION

Over the past two decades, the technological advances of device fabrication and semiconductor growth techniques have made possible the studies of small and impurity-free electron systems. At sufficiently low temperatures both the elastic mean free path and the phase coherence length become larger than the characteristic length scales of the sample, and its transport properties[1] can reveal pronounced quantum interference effects. A device, particularly well suited for studies of these effects, is the quantum dot[2] created by electrostatical lateral confinement of a two-dimensional electron gas (2DEG). The size and shape of the dot can be changed by varying the voltage of the electrodes, which determine the confining potential, thus providing a possibility to modify the system *in situ*. In ballistic quantum dots, where the boundary of the confining potential has a shape, that generates chaotic classical dynamics, one observes random, reproducible conductance fluctuations, provided the Fermi wavelength λ_F is small compared to the dot size.[1] For small dots, where this requirement is not quite fulfilled, the wave nature of the electrons reduces the sensitivity to the initial conditions characteristic of chaotic dynamics, and a more regular electronic motion appears. Recently, the attention has turned towards quantum dots that are just marginally chaotic, i.e., devices capable of showing both regular and chaotic behavior described by a mixed phase space.[2–9]

Besides the size and overall shape of the potential, the leads feeding current into the quantum dot are often perturbations on an intentionally regular confining potential. As the leads are gradually opened, the dynamics therefore changes from regular to chaotic.[10] Furthermore, it is expected theoretically[11] that the total phase breaking rate $\tau_\phi^{-1} + \tau_{esc}^{-1}$ is enhanced, as escaped electrons are reinjected with uncorrelated phases. As the leads are opened, the quantum dot is no longer an isolated system, its eigenstates become lifetime broadened, and in the limit of wide open leads they eventually evolve into scattering resonances in a continuous spectrum. In transport measurements this allows only the gross shell structure rather than individual levels to be resolved.[6]

Several observations of periodic magnetoconductance fluctuations in open dots have been interpreted semiclassically, based on periodic orbits, or quantum-mechanically, based on scarred wave functions.[2–4,6–9] The observed periods ΔB in magnetic field can be related to the area F encompassed by a periodic orbit using the Aharanov-Bohm type relation $F\Delta B = \Phi_0$, where $\Phi_0 = h/e$ is the flux quantum. This relation and generalizations thereof can be more rigorously obtained from semiclassical periodic orbit theory.[12] In the spirit of Bohr and Sommerfelds quantization rule, periodic orbit theory provides a connection between the classical action of the periodic orbits and the density of states in the quantum regime.

When analyzing the experimental results, however, the resolution seldom warrants an interpretation in terms of the full periodic orbit theory: to extract the quantum density of states from the transport measurements is a difficult, if not impossible task. This is also the case for our work, so to explain the quasiperiodic magnetoconductance fluctuations observed for our triangular dots, we simply start from the classical action of a periodic electron orbit of length L encompassing an area F, which for a constant wavelength λ_F becomes

$$N = \frac{1}{h} \oint (\mathbf{p} - e\mathbf{A}) \cdot d\mathbf{q} = \frac{L}{\lambda_F} - \frac{BF}{\Phi_0}. \tag{1}$$

This yields a magnetic field-dependent quasiperiod $\Delta B(B)$ given by

$$\Delta B(B) = \left| \frac{dN}{dB} \right|^{-1}, \tag{2}$$

since both L and F depend on the magnetic field. In most experiments such an oscillation has to be extracted from a complicated background consisting of additional periodic components as well as an aperiodic part.[3]

The role of leads as selective probes of resonant states has recently been emphasized.[7–9] The collimated beam of electrons injected through one lead selects a set of momenta and coordinates, i.e., a particular part of phase space. Semiclas-

sically, resonances occur when the direct trajectories are being injected close to periodic orbits in phase space.

In this work we focus on the role of leads for providing a mechanism to select periodic orbits in quantum dots with mixed dynamics, and we have chosen a triangular geometry of the dot to obtain a particularly simple set of periodic orbits. In Sec. II we describe the experiment and a simple geometrical model for the electrostatic potential induced by the gates. Then, in Sec. III we use classical simulations to assert that the periodic fluctuations in the low-temperature magnetoconductance are not of classical origin. In Sec. IV we compare the measured quasiperiod of the quantum oscillations to the results of a numerical and analytical analysis of the classical trajectories. We show that particularly robust and strong conductance oscillations can be related to a single orbit that is classically inaccessible from the leads. Finally, in Sec. V we discuss the origin and the implications of the small coupling between this periodic orbit and the leads. It is concluded that selective probing is not necessary to detect periodic orbits in a small, open cavity with mixed dynamics.

II. EXPERIMENT

A GaAs-Al$_x$Ga$_{1-x}$As heterostructure with a 2DEG embedded 90 nm under the surface is used as a starting point for the device fabrication. The mobility of the 2DEG after processing is about 200 m^2/V s and the carrier density 1.7 $\times 10^{15}$ m^{-2}. Using electron-beam lithography, three hexagonal aluminum gates are deposited on the surface of the heterostructure, as shown in the insets of Fig. 2. By applying a negative gate voltage of -0.3 V, an equilateral triangular cavity with open corners is formed between the gates. We present measurements performed on three samples, in the following referred to as A1, A2, and B1. Samples A1 and A2 are nominally identical while sample B1 has the same lithographic shape, but an area twice as large. The lithographic width W of the leads is 0.39 μm for sample B1 and 0.27 μm for samples A1 and A2. The corresponding pinch-off voltages for the three samples are $V_{B1} = -1.0$ V, $V_{A1} = -0.50$ V, and $V_{A2} = -0.57$ V. The side length of the hexagonal gates is $2W$ in all samples. Based on the classical ballistic features described in Sec. III, we find the carrier densities to range between 0.7 and 1.0 in units of 10^{15} m^{-2} for all confined quantum dots, corresponding to a Fermi wavelength $\lambda_F \approx 80$ nm.

The electrostatic potential changes the area and shape of the dot significantly from the first formation to pinch off. In the analysis of our data, we therefore need to estimate the size of the dot as a function of gate voltage. When the dot is formed at the gate voltage $V_d = -0.3$ V, the edge of the electron gas is assumed to be directly under the edge of the gates. As the gate voltage is made more negative, a region of width d is depleted around the gates, until the three point contact regions are fully depleted at the pinch-off voltage V_p. In a theoretical study of a half plane gate situated in the plane of a 2DEG, Shikin and Larkin[13] found a linear relation between the depletion width d and the gate voltage V_g. The depletion zone around one of the hexagonal gates is assumed to be independent of the two other gates, and consequently the dot shrinks linearly from the lithographic shape at $V_g = V_d$ to a smaller triangle near pinch off at $V_g = V_p$. We can

now express the area F of the dot as a function of the gate voltage, or more conveniently as a function of the dimensionless gate voltage $\widetilde{V} = (V_g - V_d)/(V_p - V_d)$ as follows: $F_{\text{dot}} \approx W^2(\sqrt{3}/4)[(4 - 3\widetilde{V}/2)^2 - 3(1 - \widetilde{V})^2]$. With this model we estimate the areas 0.41 μm^2 (0.83 μm^2) for sample A1 (B1) at the formation of the dots, and roughly half these areas near pinch off.

The samples are cooled to 20 mK in a dilution fridge located in a rf-shielded room. Using standard lock-in techniques the three-terminal devices are measured in a current-biased two-probe configuration with the third probe floating. Excitation currents are typically 1 nA at an ac frequency of 117 Hz. Despite filtering, the electron gas is not cooled below 50 mK, as estimated from the activated behavior of the resistivity ρ_{xx} on the $\nu = 2/3$ fractional quantum Hall plateau and from the temperature dependence of the low field conductance fluctuations. The magnetic field sweep rate dB/dt was kept below 0.15 T/min to avoid additional heating due to eddy currents.

III. CLASSICAL EFFECTS

Before studying the quantum interference effects, we first have to identify those parts of the conductance fluctuations, which are related to purely classical effects. One possible way to discern classical conductance variations from quantum fluctuations is to increase the temperature. The classical variations are far less temperature dependent than the quantum fluctuations, reflecting the elastic mean free path being less temperature dependent than the phase-breaking length.[1,2] Above 1 K the quantum fluctuations are largely suppressed, and we are left with the classical variations, which for sample A1 near pinch off are dominated by a large conductance dip around zero field as shown in Fig. 1. This zero field dip is quite large (of the order of e^2/h), is accompanied by two smaller conductance maxima at 0.11 and 0.35 T. We find this overall shape and field scale of the magnetoconductance preserved up to about 10 K, where the variations vanish due to the increased scattering.[14] Similar behavior is observed for samples A2 and B1.

To identify the classical ballistic part of the conductance, we performed a semiclassical simulation in a potential resembling the effective potential of the cavity, and compared the calculated conductance to low- and intermediate-temperature measurements. The advantage of this approach is twofold: it allows us to gain an understanding of the physics behind the conductance variations in the classical regime and it provides a way to make consistent deductions on the shape of the effective potential and the carrier density in the dot, as these two parameters determine the amplitude, shape, and field scale of the magnetoconductance variations. The four steps of our analysis are straightforward. (1) A soft model potential is defined on a lattice, allowing us to calculate the force on each point in the xy plane. (2) An ensemble of electrons is injected with cosine distributed angles in lead $i = 1$, and tracked to the exit leads $j = 1,2,3$ using the classical equations of motion. (3) The transmission coefficients T_{ji} are calculated as the number of modes in lead i times the probability of ending in lead j when starting from lead i. (4) Using Landauer-Büttiker formalism for a three probe dot with triangular symmetry,[15] the conductance becomes
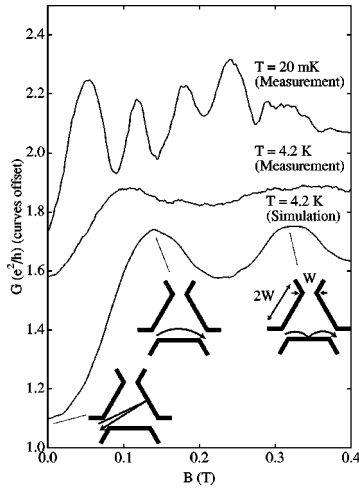
FIG. 1. Magnetoconductance of sample A1 at $T = 20$ mK (top) and $T = 4.2$ K (middle) compared to the result of a classical simulation involving 20 000 injected particles per data point (bottom), with energies distributed according to the temperature $T = 4.2$ K. The model potential is a step potential shaped like the gates but softened by a Gaussian function of width $\gamma = 45$ nm. The carrier density is 0.7×10^{15} m^{-2}. We note that the same choice of parameters yields the fit of the quasiperiods in Fig. 3(c). The insets schematically show the origin of the variations: the main dip is related to backscattered trajectories, whereas the two conductance maxima correspond to direct transmission and a single skipping orbit.

$G_{12,12} = (2e^2/h)(T_{21} + T_{31}^2/[T_{21} + T_{31}])$, where the triangular symmetry conditions $T_{12} = T_{23} = T_{31}$ and $T_{13} = T_{21} = T_{32}$ are used.[14]

We have used two model potentials. First, the threefold Hénon-Heiles potential[12,16] with appropriately chosen parameters, which in polar coordinates has the form $U(r, \theta) = \alpha r^2 + \beta r^3 \sin(3\theta)$ and secondly, a gate-shaped step function ($U = V_g$ on the gates and $U = 0$ between the gates), convoluted by a Gaussian function of width γ to emulate the soft walls characteristic of electrostatic potentials.[13] By changing the smoothing width γ the convoluted potential can be varied from being nearly hard walled, $\gamma \simeq 0$, to being very soft walled, $\gamma \gg W$. For $0 < \gamma < W/2$ the potential is fairly hard walled with corresponding flat regions in the center at distances roughly greater than γ away from the gates. In contrast, the Hénon-Heiles potential always has a soft parabolic shape in the center.

In Fig. 1 we compare the magnetoresistance traces of sample A1 close to pinch off at temperatures $T = 4.2$ K and $T = 0.02$ K with a numerical 4.2 K simulation. For each calculated value $G(B)$, 20 000 trajectories with energies distributed according to the finite temperature are started outside the cavity, the majority being backscattered before entering the dot. We find fair agreement between measurement and simulation by choosing rather hard walls with a smoothing width γ of only 45 nm, and by choosing a carrier density $n = 0.7 \times 10^{15}$ m^{-2}. The measured conductance variations in Fig. 1 are smaller than observed in the simulation, which we believe is due to temperature-induced scattering processes not taken into account; at 8 K the classical variations are nearly washed out. The simulation could probably be further improved using a self-consistent potential such as in Ref. 17. However, the same values used for γ and n in the simple
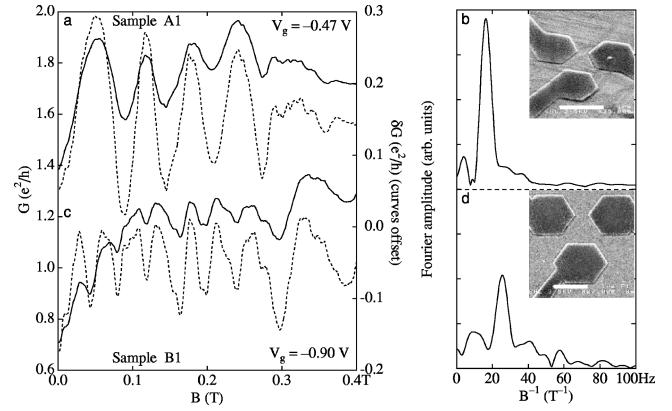

FIG. 2. At low temperatures the magnetoconductance traces exhibit an oscillatory structure up to roughly 0.3 T (sample B1) and 0.4 T (sample A1), which is considerably stronger than random conductance fluctuations. Panel (a) shows for sample A1 the raw conductance measurement (full curve) and the measurement with the classical background filtered out (dashed curve), while panel (b) shows the corresponding power spectrum ($0 < B < 0.3$ T). Accordingly, panels (c) and (d) show conductance and power spectra for sample B1. For the small dot A1, the oscillations are almost free of other harmonics, whereas sample B1 exhibits more frequencies. For sample A1, the oscillations die out at higher fields than for sample B1, and persist over a larger range of gate voltage. The insets in the power spectra show SEM micrographs of the samples with white bars of length 1 μm.

simulation presented in Fig. 1 also lead to an excellent agreement for the quasiperiod as shown in Fig. 3(c) to be discussed in Sec. IV. We therefore conclude that the simulation works satisfactorily, and it shows that the conductance dip around $B = 0$ T is caused by trajectories reflected by the flat wall opposing the source lead. As the magnetic field is increased to $B \approx 0.1$ T, the collimated electron beam is directed into the exit lead, leading to a maximum in the conductance. A similar peak is seen at $B \approx 0.3$ T, where the trajectories perform one bounce on the edge of the potential before exiting. Similar geometric resonances have been studied in semiconductor double slits,[18] in rectangular cavities,[8,19] and in etched triangular cavities.[9]

We conclude that the slow variations in the magnetoconductance at intermediate temperatures are of classical nature containing no oscillatory structure on scales smaller than 0.1 T. We have estimated n to be between 0.7 and 1.0 in units of 10^{15} m^{-2} and found evidence for the effective potential being fairly hard walled and therefore quite far from the Hénon-Heiles type. As we now have accounted for the conductance features seen at intermediate temperatures we now proceed to the low-temperature regime.

IV. QUANTUM INTERFERENCE EFFECTS

In all samples we find pronounced oscillatory structure in the magnetoconductance below 1 K in addition to the slow variations at higher temperatures. As seen in Fig. 1 the low-temperature conductance oscillations in sample A1 completely dominate the classical conductance variations, making the classical background difficult to observe. In Fig. 2 the magnetoconductance data of samples A1 and B1 are shown before (full lines) and after (dashed lines) applying a high

pass filter to remove the relatively slow classical variations.

The oscillations in the smaller samples of type A are generally twice as strong as in the larger samples of type B, they also persist over larger ranges of gate voltages, and they tend to be dominated by a single quasiperiod with little other structure. The main oscillation of sample B1 is accompanied by other periodic and aperiodic components. The dominating periods measured in sample A1 (40–70 mT) are larger than those in sample B1 (25–40 mT). The peak positions generally move as the size of the quantum dot is changed, i.e., by varying the gate voltage. We point out that the samples A1 and A2 are not identical, and that the same sample behaves differently from cool down to cool down. The overall behavior is, however, conserved. The oscillations continue with roughly constant quasiperiod up to about 0.3 T in all three samples, as reflected in the narrow peaks in the power spectra shown in Figs. 2(b) and 2(d). Above this field, the fluctuations become weaker while the quasiperiod (peak-to-peak distance) increases. In all cases the oscillations remain essentially unchanged on a time scale of 24 h, except for minor differences in shape due to occasional redistribution of the potential, presumably caused by charge hopping between the donor atoms in the GaAlAs barrier layer.[17]

The presence of a single quasiperiod over a range of magnetic fields and gate voltages implies the existence of a single orbit which is robust to both changes in magnetic field and the shape of the potential. By analyzing the classical trajectories in soft- and hard-walled model potentials and homogeneous magnetic fields (see Sec. II), we note that the triangular loop orbit with the same winding direction as the free electron cyclotron orbit is the only orbit which exists in the large field range of the experimentally observed oscillations. Rather than being destroyed as the magnetic field is augmented, it gradually changes into the cyclotron orbit which is also a single loop. The triangular orbit at low fields can therefore be seen as a cyclotron orbit forced to fit inside the triangular cavity. Indeed, a detailed analysis of the observed magnetoconductance reveals a smooth transition from the low field oscillations with a nearly constant quasiperiod, to Landau level quantization oscillations, or Shubnikov–de Haas oscillations, periodic in B^{-1}. This is shown in Fig. 3. In panel (a) is displayed a gray-scale plot of the conductance as a function of both magnetic field B and gate voltage V_g. It is clearly seen how the resolved oscillations are of the B^{-1} periodic Shubnikov–de Haas type in the open quantum dot [$V_g \approx -0.27$ V, top of panel (a)], where the magnetic confinement dominates the electrostatic confinement already when the first oscillation can be resolved. This is in contrast to the nearly closed quantum dot [$V_g \approx -0.55$ V, bottom of panel (a)], where a more constant quasiperiod is seen at low fields before the B^{-1} periodic behavior sets in. In the regime between the two limits ($G \sim e^2/h$ and $G \gg e^2/h$) where several conducting channels are passed through the system, the fluctuations are generally less clear, and at some gate voltages practically disappear.

In Figs. 3(b) and 3(c) the results of a quantitative analysis are shown. We begin by considering the triangular periodic orbit in a hard-walled potential, where it in zero field is an equilateral triangle.[20] In weak fields, the triangular orbit splits into two orbits: a large area orbit ($+$) winding the same way as the cyclotron orbit, and a smaller area orbit
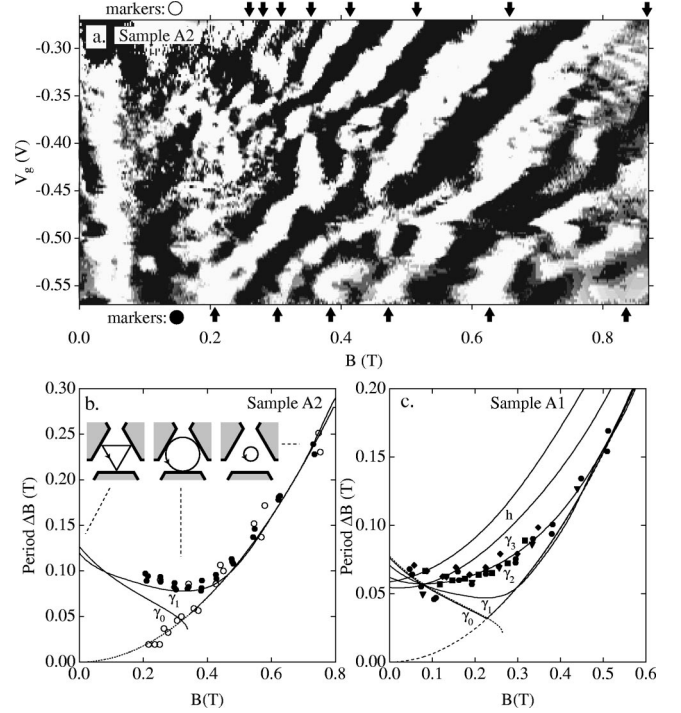

FIG. 3. Panel (a) shows the conductance of sample A2 in a gray-scale plot (bright denotes low conductance), versus gate voltage and magnetic field. The gate voltage ranges from -0.27 V (formation point), to the pinch-off voltage -0.57 V for this particular dot. The arrows at the top of the graph show the conductance maxima being periodic in B^{-1} characteristic of Landau level (LL) oscillations in an electron system with carrier density of 1.0×10^{15} m^{-2}. The arrows at the bottom show the B quasiperiodic oscillations related to the triangular loop orbit, with an increasing quasiperiod at high fields. In panel (b) the measured quasiperiods of sample A2 are compared to the analytical expression Eq. (6) for a hard-wall potential (γ_0), as well as numerical calculations for a step potential with soft region width of 15 nm (γ_1). The best fit is obtained by choosing the carrier density $n_{A2}=1.0\times10^{15}$ m^{-2}. The white markers show the measured oscillation quasiperiods of the sample at the point of formation being $1/B$ periodic, down to much lower fields than when the dot is near pinch off (black markers). Similarly, in panel (c) results for the quasiperiod of sample A1 are compared to the analytical expression Eq. (6) for a hard wall potential (γ_0), as well as numerical calculations for step potentials with soft region widths of 15 nm (γ_1), 45 nm (γ_2), and 73 nm (γ_3). The top curve (h) shows the calculation for the Hénon-Heiles potential. As in Fig. 1 the γ_2 potential matches the data best together with a carrier density $n_{A1}=0.7\times10^{15}$ m^{-2}.

($-$) winding the opposite way. Between the reflections at the walls of the quantum dot, the electrons move on arcs with the cyclotron radius $R_c = \hbar k_F / eB$. For weak magnetic fields a p-corner periodic orbit exists in any regular p-sided polygonal potential with hard walls, as for instance seen in Ref. 7. In soft potentials, the corners of the orbit will be rounded accordingly. In terms of the dimensionless magnetic field $b = l_0/2R_c$ the field-dependent length $L(b)$ and area $F_\pm(b)$ of a p-corner periodic orbit, which at zero field has sidelength l_0 can be written as

$$L(b) = \frac{pl_0}{b}\arcsin(b), \qquad (3)$$

$$F_{\pm}(b) = \frac{p l_0^2}{4} \left[\pm \cot\left(\frac{\pi}{p}\right) + \frac{\arcsin(b)}{b^2} - \frac{\sqrt{1-b^2}}{b} \right]. \quad (4)$$

By inserting these equations into Eq. (1) the quantization rule becomes

$$N_{\pm} = \frac{p l_0}{2\lambda_F} \left[\mp b \, \cot\left(\frac{\pi}{p}\right) + \frac{1}{b} \arcsin(b) + \sqrt{1-b^2} \right], \quad (5)$$

where N_+ (N_-) is the orbit winding the same (opposite) way as the cyclotron orbit. The corresponding magnetic-field-dependent quasiperiods $\Delta B_{\pm} = |dN_{\pm}/dB|^{-1}$ are then given by

$$\Delta B_{\pm} = \frac{4\Phi_0}{p l_0^2} \left| \mp \cot\left(\frac{\pi}{p}\right) - \frac{\arcsin(b)}{b^2} + \frac{\sqrt{1-b^2}}{b} \right|^{-1}. \quad (6)$$

By comparison with Eq. (4) it is seen that the quasiperiod of the (+) orbit takes on the simple form $\Delta B_+ = \Phi_0/F+(b)$. Above a certain field strength $b^* = \sin(\pi/p)$, where the cyclotron radius R_c is equal to the radius of the circumscribed circle, the (+) orbit is just the cyclotron orbit. We note that the Landau level filling factor $\nu = n\Phi_0/B$ can be derived semiclassically by applying the Bohr-Sommerfeld quantization rule Eq. (1) to the cyclotron orbit, giving $N_{\mathrm{LL}} = \nu/2$ with the factor of 2 due to spin degeneracy. The corresponding quasiperiod ΔB_{LL} is then quadratic in b (see Fig. 3):

$$\Delta B_{\mathrm{LL}} = \frac{2B^2}{n\Phi_0} = \frac{4\Phi_0}{\pi l_0^2} b^2. \quad (7)$$

The (−) orbit exists only at low fields $b < 1$, and furthermore its quasiperiod diverges at $b = 1$ around 0.2 T, which disqualifies it as an explanation for the observed oscillations. We apply Eq. (6) for $b < b^*$ and Eq. (7) for $b > b^*$ to our system by setting $p = 3$ (triangular orbit) and by using the geometrical relation $l_0 = (2 - 0.75\tilde{V})W$ for the zero-field orbit side length as a function of the dimensionless gate voltage $\tilde{V}$ (see Sec. II).

In Fig. 3(b) the calculated hard-wall quasiperiod denoted γ_0 is plotted against magnetic field B together with measured periods (black markers) of conductance oscillations in sample A2 and similarly in Fig. 3(c) for sample A1. The measured periods represent the distance between adjacent maxima (or minima) of quasiperiodic oscillations plotted at the fields halfway between the maxima (or minima). The transition to a cyclotron orbit is taking place at the sharp minimum of the curve. In a more accurate quantum-mechanical calculation, this minimum would be smoothed, as the transition from one type of orbit to another is continuous due to the finite extent of the wave function by which the hard wall appears more soft.[21] Likewise, classically the hard-wall model predicts much larger variations of the quasiperiod $\Delta B(B)$ in the low field region, than obtained with softened walls. Therefore, to improve the hard-wall model we calculate the quasiperiod $|dN/dB|^{-1}$ numerically for the sequence of loop orbits that exist in soft potentials in the field range from zero to 0.8 T. By this we not only obtain a closer match to the actual potential, we also avoid the above mentioned discontinuities in the transition from the triangular to the circular orbit.
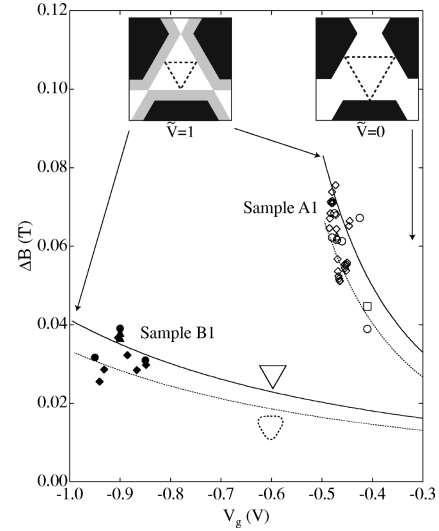

FIG. 4. The measured quasiperiods determined from the power spectra of seven measurement series plotted together with the calculated quasiperiod corresponding to the triangular orbits. For comparison, the areas of the softened triangles, as estimated from numerical calculations, are indicated by the dotted lines.

In Figs. 3(b) and 3(c) we plot in addition to the analytical predictions of Eqs. (6) and (7), the periods obtained numerically with the Hénon-Heiles potential (h) and three step potentials, $\gamma_1 - \gamma_3$, of different smoothing widths γ. Again we obtain the best agreement with the fairly steep potentials softened only a little by choosing the same small values of γ and the same carrier density n as in Sec. III.

We note from the simulations that the soft walls tend to stabilize the quasiperiod of the (+) orbit at low fields, and that the simple relation $\Delta B_+ = \Phi_0/F(b)$ found for hard walls is approximately correct for softened walls as well. The field dependence of the quasiperiod related to the triangular orbit then turns out to be similar to that of an orbit with constant area and length. These facts allow us to use the zero field triangular orbit in the further analysis of oscillations at low fields. With the linear depletion model of the dot (see Sec. II) we obtain the following approximative expression for the area of the triangular orbit as a function of the dimensionless gate voltage $\tilde{V}$:

$$F_{\triangle}(\tilde{V}) \simeq W^2(0.24\tilde{V}^2 - 1.30\tilde{V} + 1.73). \quad (8)$$

Equation (8) contains no adjustable parameters; it is based on the linear depletion model and the measured data. In Fig. 4 is shown that the theoretical prediction of the oscillation periods $\Delta B = \Phi_0/F_{\triangle}$ as a function of the gate voltage V_g is in good agreement with the experimental data points. The fact that the measured periods are slightly smaller than predicted is due to the hard wall triangle being slightly smaller in area than its soft wall rounded counterpart. From the simulations we estimated the difference in area to be roughly 20%, which leads to the corrected curves (dotted) in Fig. 4.

Finally, we observe an almost complete suppression of random fluctuations in the oscillatory regime, which is clear from the isolated peaks in the power spectra of Fig. 2. A possible factor to the suppression of random fluctuations is the small ratio between size and wavelength caused by the
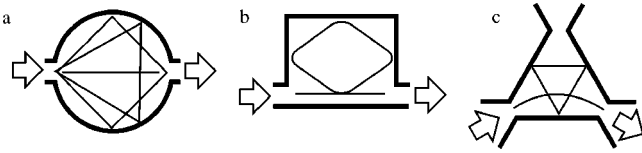
FIG. 5. Panels (a) and (b) show the geometries discussed by Persson (Ref. 6) and Bird (Ref. 7) (see text). Some periodic orbits related to the conductance oscillations observed in the samples are sketched. In both cases the collimated beam can inject close to a periodic orbit in phase space. In panel (c) the triangular sample is sketched. The incoming orbit does not match the direction of the triangular orbit anywhere; this orbit is classically inaccessible in phase space, in contrast to the situation shown in panels (a) and (b).

low carrier densities. When sample A1 is smallest (near pinch off), the length of the symmetry axis from gate to lead is about 6 times the Fermi wavelength $\lambda_F = 80$ nm, while the total length L of the triangular orbit is $10\lambda_F$, compared to roughly $18\lambda_F$ for the square orbit considered in Ref. 7. The small sample A1 does not quite fulfill the condition $\lambda_F \ll L$ and random fluctuations are suppressed.

V. DISCUSSION

Having established that the low field conductance oscillations are due to the triangular periodic orbit, which changes into a cyclotron orbit at high fields, we discuss qualitatively the coupling between the incoming electrons and the orbit causing the conductance oscillations.

Recently, quasiperiodic magnetoconductance oscillations in square and triangular quantum dots have been interpreted in terms of selective probing[7–9] where the incoming electrons are injected close to the classically periodic orbits as sketched in Figs. 5(a) and 5(b). The same interpretation may in fact also be applied to circular dots.[3,6,22] A common feature of these billiard shapes is that the polygons accessible from the leads are single members of families of degenerate orbits with the same classical action. As an example, in the circular case these are rotated copies of the accessed polygon. Classically, small-angle scattering can transfer a particle from one orbit (or family) to another until it finally couples to the lead and escapes. The situation for our triangular samples is entirely different: the orientation of the triangular loop orbit is fixed with respect to the leads, and the orbit is isolated, i.e., it does not belong to any continuous family of orbits. As illustrated in Fig. 5(c), the incoming electron beam does not inject into the loop orbit. From the analysis of the classical dynamics, we have noted that just a small fraction of injected electrons end up in trajectories close to the loop orbit at small fields, $B < 0.15$ T, and none at higher fields, where the loop orbit is localized in the center of the dot. So even if the quasiperiod of the oscillations can be explained in terms of one periodic orbit, the coupling between the incoming trajectories and the periodic orbit is expected *a priori* to be weak. However, we will argue that the remarkable robustness and strength of the observed oscillations is exactly a consequence of this weak coupling. In a sense the triangular orbit resembles a resonating oscillator only weakly coupled to the surroundings, but the weak coupling translates into a high Q value with a significant response as a consequence in steady state.

Quantum mechanically the spatial structure of high-lying eigenstates often resembles periodic orbits of the corresponding classical system. In the semiclassical limit, i.e., for mesoscopic systems, these so-called scarred wave functions are particularly important.[7–9,12] We speculate that the triangular orbit in our system is largely represented by a set of scarred wave functions similar to those found also in a triangular quantum dot.[9] In that study, however, a different lead geometry implies a strong coupling between the periodic orbits and the leads. It is possible to explain the weak coupling found in our classical simulation by noting that the propagation direction of the incoming wave will be almost orthogonal with the scarred wave function propagating along the triangular orbit thus yielding an almost vanishing overlap integral. The experimental evidence of a nonzero coupling would then be a manifestation of quantum mechanical tunneling in phase space without classical counterparts.[6,23] A similar situation has been seen in the high field Aharonov-Bohm effect in quantum dots,[24] where the outer edge state propagates through the dot while the inner edge state is an isolated loop. In this case, tunneling into the inner state leads to magnetoconductance oscillations corresponding to the area of the inner isolated state. In the wave picture, as in the classical picture, the remarkable robustness and strength of the observed oscillations can be explained in terms of high Q values: once a wave packet is launched along the isolated triangular orbit, small-angle scattering cannot bring it close to an exit lead; only a tunneling process in phase space can do so. The triangular orbit acts as a wave resonator with a high Q value, and we come to the surprising conclusion that periodic orbits can be observed most clearly in those transport measurements where the orbits in question are not directly accessible to the incoming particles injected from the leads but in fact are only weakly coupled to the leads.

As a final remark we note that the smooth transition from oscillations in B to oscillations in $1/B$ indicates that the low field oscillations is a density of states effect similar to Landau quantization, and that the main difference between the two field regimes is whether the confinement is of electrostatic or magnetic origin. Loosely speaking, the density of states from the inner dot contributes significantly to the scattering resonances, and the conductance oscillations can be interpreted as a manifestation of gross-shell structure in the energy spectrum related to the existence of periodic orbits.[12] A consequence of the appearance of such a gross-shell structure would be that the thermal behavior of the fluctuation amplitude differs from those of chaotic energy spectra. Due to level repulsion in a chaotic system, the typical level spacing is equal to the average level spacing $\langle \Delta \rangle$. The amplitude of the fluctuations increases with decreasing temperature, only until the thermal energy $k_B T$ becomes smaller than $\langle \Delta \rangle$, where the number of available scattering states becomes independent on the temperature. This has been seen experimentally in a system similar to ours.[25] However, for systems showing gross-shell structure the typical level spacing becomes smaller than $\langle \Delta \rangle$ due to the appearance of large gaps $\Delta_{\mathrm{gap}} > \langle \Delta \rangle$ in the energy spectrum. Saturation should then set in on the larger energy scale Δ_{gap}, giving rise to a higher saturation temperature $T \approx \Delta_{\mathrm{gap}}/k_B$.

In the smallest triangular sample A1, we observe indeed

such a saturation of $\langle \delta G \rangle$ below temperatures of 0.5 K and corresponding bias voltages eV_{bias}/k_B. This effect is not due to trivial saturation of the electron gas temperature, which only occurs at much lower temperature (~ 0.05 K). This is evident not only from resistance measurements in the fractional quantum Hall regime (see Sec. II) but also from the temperature dependence of the conductance fluctuations: the shape of the conductance fluctuations changes throughout the temperature range from 0.5 to 0.05 K, and simultaneously the correlation field as obtained from the autocorrelation of the fluctuations decreases below the transition temperature. However, applying the same analysis as in Ref. 25 to our data we obtain saturation energies 1.5 to 4 times larger than the expected value $\langle \Delta \rangle$ indicating the presence of the above-mentioned shell structure. Furthermore, we observe a tendency of the saturation to set in at higher temperatures, when the dot is near pinch off, consistent with an increased shell spacing as the dot is made smaller. If this explanation is correct, the temperature dependence of the fluctuations provides an interesting possibility of detecting the quantum properties of small cavities with mixed dynamics. We propose that the bias voltage could be used as a convenient parameter to control the thermal broadening of the levels in order to extract information on the level distribution as described above.

VI. SUMMARY

We have studied the intermediate- and low-temperature magnetoconductance of triangular symmetric quantum dots of different sizes. At low temperatures we observe strong periodic fluctuations in the magnetoconductance, which are robust to moderate variations in gate voltage and magnetic field. While the quasiperiod is nearly constant at low magnetic fields, a $1/B$ periodicity is observed at higher fields, similar to Shubnikov–de Haas oscillations. The magnetic field dependence of the oscillation periods has been analyzed numerically and analytically in terms of one classical orbit: the triangular loop orbit. To account for the effect of gate voltage on the area of the orbit we assumed linear depletion as a function of gate voltage. This leads to a geometrical model without adjustable parameters that agrees well with the measured oscillation periods obtained at different gate voltages. The orbit in question is inaccessible in terms of classical collimated trajectories, and we therefore propose that the transport mechanism is a pure quantum tunneling effect, through the essentially isolated triangular periodic orbit. The quasi-isolation of the orbit explains the robustness and strength of the observed oscillations, and our work has led us to the conclusion that periodic orbits can be observed very clearly in systems where the orbits are not directly accessible to the incoming particles injected from the leads. Finally, the quasi-isolation of the triangular orbit leads to the appearance of shell effects with implications for the saturation temperature of the quantum fluctuations: we have measured a saturation temperature up to four times larger than the one expected for systems without shell structure.

[1] For reviews on mesoscopic phenomena see, e.g., C. W. J. Beenakker and H. van Houten, Solid State Phys. **44**, 1 (1991) or *Mesoscopic Phenomena in Solids*, edited by B. L. Altshuler, P. A. Lee, and R. A. Webb (Elsevier, Amsterdam, 1991).

[2] For a review on quantum dots see, e.g., the chapter by L. P. Kouwenhoven, C. M. Marcus, P. L. McEuen, S. Tarucha, R. M. Westervelt, and N. S. Wingreen, in *Mesoscopic Electron Transport*, edited by L. L. Sohn, L. P. Kouwenhoven, and G. Schön (Kluwer, Dordrecht, 1997).

[3] C. M. Marcus, A. J. Rimberg, R. M. Westervelt, P. F. Hopkins, and A. C. Gossard, Phys. Rev. Lett. **69**, 506 (1992).

[4] A. M. Chang, H. U. Baranger, L. N. Pfeiffer, and K. W. West, Phys. Rev. Lett. **73**, 2111 (1994).

[5] H. Bruus and A. D. Stone, Phys. Rev. B **50**, 18 275 (1994).

[6] M. Persson, J. Petterson, B. von Sydow, P. E. Lindelof, A. Kristensen, and K. F. Berggren, Phys. Rev. B **52**, 8921 (1995); K. F. Berggren, Zhen-Li Ji, and T. Lundberg, *ibid.* **54**, 11 612 (1996); S. M. Reimann, M. Persson, P. E. Lindelof, and M. Brack, Z. Phys. B **101**, 377 (1996).

[7] J. P. Bird, D. K. Ferry, R. Akis, Y. Ochiai, K. Ishibashi, Y. Aoyagi, and T. Sugano, Europhys. Lett. **35**, 529 (1996); R. Akis, D. K. Ferry, and J. P. Bird, Phys. Rev. B **54**, 17 705 (1996).

[8] I. V. Zozoulenko, R. Schuster, K. F. Berggren, and K. Ensslin, Phys. Rev. B **55**, 10 209 (1997).

[9] L. Christensson, H. Linke, P. Omling, P. E. Lindelof, I. V. Zozoulenko, and K.-F. Berggren, Phys. Rev. B **57**, 12 306 (1998).

[10] J. P. Bird, D. M. Olatona, R. Newbury, R. P. Taylor, K. Ishibashi, M. Stopa, Y. Aoyagi, T. Sugano, and Y. Ochiai, Phys. Rev. B **52**, 14 336 (1995).

[11] M. Büttiker, Phys. Rev. B **33**, 3020 (1986).

[12] For reviews on semiclassical theory see, e.g., M. C. Gutzwiller, *Chaos in Classical and Quantum Mechanics* (Springer-Verlag, New York, 1990) or M. Brack and R. K. Bhaduri, *Semiclassical Physics* (Addison-Wesley, New York, 1997).

[13] I. A. Larkin and V. B. Shikin, Phys. Lett. A **151**, 335 (1990).

[14] P. Bøggild, A. Kristensen, P. E. Lindelof, S. M. Reimann, C. B. Sørensen, and M. Persson (unpublished).

[15] C. M. Marcus, R. M. Westervelt, P. F. Hopkins, and A. C. Gossard, Phys. Rev. B **48**, 2460 (1993); H. U. Baranger and P. A. Mello, *ibid.* **51**, 4703 (1995).

[16] M. Brack, R. K. Bhaduri, C. Maier, and M. V. N. Murthy, Phys. Rev. Lett. **70**, 568 (1993).

[17] M. Stopa, Phys. Rev. B **54**, 13 767 (1996).

[18] H. van Houten, C. W. J. Beenakker, J. G. Williamson, M. E. Broekaart, and P. H. M. van Loosdrecht, Phys. Rev. B **39**, 8556 (1989).

[19] P. Bøggild, P. Hullmann, A. Kristensen, P. E. Lindelof, and S. M. Reimann, *Proceedings of LT21*, 1996 [Czech. J. Phys. **46**, 2299 (1996)].

[20] M. Brack, J. Blaschke, S. C. Creagh, A. G. Magner, P. Meier, and S. M. Reimann, Z. Phys. D **40**, 276 (1997).

[21] J. Blaschke and M. Brack, Phys. Rev. A **56**, 182 (1997).

[22] M. J. Berry, J. A. Katine, R. M. Westervelt, and A. C. Gossard, Phys. Rev. B **50**, 17 721 (1994).

[23] O. Bohigas, D. Boosé, R. Egydio de Carvalho, and V. Marvulle, Nucl. Phys. A **560**, 197 (1993).

[24] B. J. van Wees, L. P. Kouwenhoven, C. J. P. M. Harmans, J. G. Williamson, C. E. Timmering, M. E. I. Broekaart, C. T. Foxon, and J. J. Harris, Phys. Rev. Lett. **62**, 2523 (1989).

[25] J. P. Bird, K. Ishibashi, D. K. Ferry, Y. Ochiai, Y. Aoyagi, and T. Sugano, Phys. Rev. B **51**, 18 037 (1995).